Lithium solvation in dimethyl sulfoxide-acetonitrile mixtures

Rocío Semino, Gervasio Zaldívar, Ernesto J. Calvo, and Daniel Laria

Citation: The Journal of Chemical Physics **141**, 214509 (2014); doi: 10.1063/1.4902837
View online: http://dx.doi.org/10.1063/1.4902837
View Table of Contents: http://scitation.aip.org/content/aip/journal/jcp/141/21?ver=pdfcov
Published by the AIP Publishing

Articles you may be interested in

Solvation dynamics of tryptophan in water-dimethyl sulfoxide binary mixture: In search of molecular origin of composition dependent multiple anomalies
J. Chem. Phys. **139**, 034308 (2013); 10.1063/1.4813417

Coupled-cluster, Möller Plesset (MP2), density fitted local MP2, and density functional theory examination of the energetic and structural features of hydrophobic solvation: Water and pentane
J. Chem. Phys. **136**, 054305 (2012); 10.1063/1.3679933

Preferential solvation of spherical ions in binary DMSO/benzene mixtures
J. Chem. Phys. **130**, 024504 (2009); 10.1063/1.3010707

Advanced dielectric continuum model of preferential solvation
J. Chem. Phys. **130**, 024505 (2009); 10.1063/1.3010706

Molecular dynamics simulations of acetonitrile/dimethyl sulfoxide liquid mixtures
J. Chem. Phys. **120**, 4860 (2004); 10.1063/1.1644540

This article is copyrighted as indicated in the article. Reuse of AIP content is subject to the terms at: http://scitation.aip.org/termsconditions. Downloaded to IP: 157.92.4.6 On: Fri, 05 Dec 2014 14:42:06

Lithium solvation in dimethyl sulfoxide-acetonitrile mixtures

Rocío Semino,[1] Gervasio Zaldívar,[1] Ernesto J. Calvo,[1] and Daniel Laria[1,2,a)]
[1]*Departamento de Química Inorgánica Analítica y Química-Física e INQUIMAE, Facultad de Ciencias Exactas y Naturales, Universidad de Buenos Aires, Ciudad Universitaria, Pabellón II, 1428 Buenos Aires, Argentina*
[2]*Departamento de Física de la Materia Condensada, Comisión Nacional de Energía Atómica, Avenida Libertador 8250, 1429 Buenos Aires, Argentina*

(Received 27 August 2014; accepted 17 November 2014; published online 5 December 2014)

We present molecular dynamics simulation results pertaining to the solvation of Li^+ in dimethyl sulfoxide-acetonitrile binary mixtures. The results are potentially relevant in the design of Li-air batteries that rely on aprotic mixtures as solvent media. To analyze effects derived from differences in ionic size and charge sign, the solvation of Li^+ is compared to the ones observed for infinitely diluted K^+ and Cl^- species, in similar solutions. At all compositions, the cations are preferentially solvated by dimethyl sulfoxide. Contrasting, the first solvation shell of Cl^- shows a gradual modification in its composition, which varies linearly with the global concentrations of the two solvents in the mixtures. Moreover, the energetics of the solvation, described in terms of the corresponding solute-solvent coupling, presents a clear non-ideal concentration dependence. Similar nonlinear trends were found for the stabilization of different ionic species in solution, compared to the ones exhibited by their electrically neutral counterparts. These tendencies account for the characteristics of the free energy associated to the stabilization of Li^+Cl^-, contact-ion-pairs in these solutions. Ionic transport is also analyzed. Dynamical results show concentration trends similar to those recently obtained from direct experimental measurements. © *2014 AIP Publishing LLC*. [http://dx.doi.org/10.1063/1.4902837]

I. INTRODUCTION

Most of the prototype electric vehicles which are currently available in the market rely on lithium-ion batteries as power sources.[1] Unfortunately, these batteries provide a very limited driving range and are very expensive to recharge. This explains the growing interest that persists in developing more competitive options. Rechargeable lithium-air batteries represent a promising alternative because of their theoretically, high specific energy density, which would stretch their durabilities, while lowering the costs.[2,3] In 1996, Abraham *et al.*[4] proposed a model lithium-air battery in which the lithium anode was in contact with an aprotic solvent electrolyte. Since then, this architecture has been widely studied because it is the only one with energy density comparable to the one relying on fossil fuels. One of the main challenges in the design of this battery version is to find appropriate aprotic solvent media.[5–13]

Recently, a dimethyl sulfoxide (DMSO) based solvent electrolyte has been proposed.[14,15] Despite its very promising characteristics, some authors have questioned its suitability, because of its oxidation to sulfone in the presence of reactive oxygen species.[16,17] However, mixtures combining DMSO with another solvent, such as acetonitrile (ACN) – a co-solvent which is stable under oxidative conditions and has the additional advantage of exhibiting high O_2 solubility – might be a good alternative.[18] In this context, it is of interest to analyze structural and dynamical characteristics of Li^+ dissolved in these binary mixtures. Several experimental and simulation studies pertaining to the solvation of lithium in pure DMSO and in pure ACN have been reported. From the structural side, ^{7}Li NMR spectroscopy experiments have shown that the first solvation shell of Li^+ is composed of four solvent molecules in both solvents.[19,20] A similar coordination number was obtained in solid phases using crystallographic techniques[21,22] and FTIR studies.[23] Kalugin and collaborators performed simulation experiments on Li^+ solvation in DMSO.[24] Two different model potentials were implemented to describe cation-solvent interactions; in both cases, their results overestimate the experimental population of nearest neighbors. On the other hand, Onthong *et al.*[25] have developed their own all-atom potential functions, based on quantum chemical calculations; their description of the lithium solvation in DMSO is in better agreement with the experimental information.[21] Computer studies concerning the solvation of simple ionic species in pure ACN have also been undertaken.[26–28] Yet, to the best of our knowledge, simulations dealing with lithium solvation in DMSO-ACN mixtures have not yet been explored. This represents the main motivation of the present paper, in which we will present results from molecular dynamics experiments that support and complement recent results obtained from rotating disc electrode studies of O_2 reduction[18] and electrochemical measurements.[29] In order to provide a broader physicochemical scenario of the ionic solvation in these solvent mixtures, we have also examined the solvation of K^+ and Cl^- to assess the importance of the effects derived from considering larger cation sizes and the asymmetries between the cationic and anionic solvations as well.

a)Author to whom correspondence should be addressed. Electronic mail: dhlaria@cnea.gov.ar

 © 2014 AIP Publishing LLC

This article is copyrighted as indicated in the article. Reuse of AIP content is subject to the terms at: http://scitation.aip.org/termsconditions. Downloaded to IP: 157.92.4.6 On: Fri, 05 Dec 2014 14:42:06

This paper is organized as follows: in Sec. II the methodology and computational details of the simulation experiments are presented. Section III includes the results of our simulations. Finally, in Sec. IV we summarize the main conclusions of this work.

II. MODEL

The systems under investigation consisted of single ions immersed in different DMSO-ACN mixtures with $x_{\mathrm{ACN}} = 0$, 0.25, 0.5, 0.75, 0.9, and 1. A few test runs were also performed at highly dilute DMSO concentrations, $x_{\mathrm{ACN}} = 0.97$. The solvents were confined in periodically replicated, cubic boxes with lengths adjusted so as to bring the global densities in agreement with experimental values.[30] In all cases, the total number of solvent molecules was fixed at 500, which corresponds to box lengths intermediate between $\ell_{\mathrm{BOX}} \sim 35$ and 40 Å. The *Packmol* package[31] was used to generate initial configurations of the mixtures. The systems were thermalized by multiple velocity rescalings, obtained from Maxwell-Boltzmann distributions at $T = 298$ K. After ∼1 ns equilibration periods, three statistically independent, 2–10 ns microcanonical production runs were carried out. In simulations with minimum content of DMSO, i.e., $x_{\mathrm{ACN}} \gtrsim 0.9$, special care was taken to avoid eventual trappings in local potential energy minima. For the latter cases, the thermalization processes involved a series of runs at $T \sim 500$ K, followed by smooth temperature ramps, down to ambient conditions. Long range interactions were treated by implementing Ewald summations using a particle mesh procedure,[32] assuming the presence of a neutralizing continuum background. Molecular dynamics simulations were performed using the *NAMD* simulation package.[33]

All molecules were modeled as flexible collections of atoms. As such, the total potential energy of the simulated systems involved intra and intermolecular contributions, namely,

$$U = U_{intra} + U_{inter}. \tag{1}$$

The intramolecular term included the standard stretching, bending, and dihedral torsion contributions

$$U_{intra} = U_{str} + U_{bnd} + U_{dih}. \tag{2}$$

The first term is a sum of interactions of the type

$$U_{str} = \sum_{\text{bonds}} k_{str}(r - r_0)^2; \tag{3}$$

where r represents the distance between pairs of nearest neighbor atoms. The bending term in Eq. (2) was considered as a sum of the type

$$U_{bnd} = \sum_{\text{angles}} k_{\theta}(\theta - \theta_0)^2; \tag{4}$$

whereas the dihedral interactions were modeled as

$$U_{dih} = \sum_{\text{dihedrals}} k_{\phi}[1 + \cos(n\phi - \delta)]. \tag{5}$$

On the other hand, the intermolecular potential energy U_{inter} was considered as a sum of site-site non-bonding interactions involving Lennard-Jones plus Coulombic terms

$$U_{inter} = \sum_{i<j} \sum_{\alpha,\gamma} u_{\alpha\gamma}\left(\left|\mathbf{r}_i^{\alpha} - \mathbf{r}_j^{\gamma}\right|\right), \tag{6}$$

with

$$u_{\alpha\gamma}(r) = 4\epsilon_{\alpha\gamma}\left[\left(\frac{\sigma_{\alpha\gamma}}{r}\right)^{12} + \left(\frac{\sigma_{\alpha\gamma}}{r}\right)^{6}\right] - \frac{z_{\alpha} z_{\gamma} e^2}{r}. \tag{7}$$

In the previous equations, $\mathbf{r}_i^{\alpha}$ and z_{α} represent the coordinate of site α in the ith molecule and its corresponding partial charge, respectively.

In recent years, several force fields have been implemented in computer simulation experiments describing liquid phases of DMSO[34–39] and ACN.[40–42] Unfortunately, for ionic solutions, all the proposed parametrizations fail to reproduce key experimental characteristics of the solvation – such as coordination numbers, for example – of small cations, such as Li^+.[24] Our strategy to tackle these problems involved looking for an optimal set of parameters that would yield structural results in agreement with previous simulation results describing ACN-DMSO mixtures[43] whereas, at the same time, would reproduce the experimental coordination numbers reported for Li^+ in pure DMSO[19,21] and in pure ACN.[20,22,23] After several attempts, we found that the combination involving the *FS* potential for DMSO reported in Ref. 38 and the "*A model*" for ACN, developed by Nikitin *et al.*,[42] along with the Li^+ parameters proposed by Dang[44] satisfied the latter requirements, provided a slight, ∼0.1 Å, reduction in the cation size is operated. A detailed list of all potential parameters implemented in the present study appears in Table I. For Lennard-Jones cross site-site interactions, we adopted the usual arithmetical and geometrical means for the establishing length and energy parameters.[45]

III. RESULTS

The starting point of our analysis will be the consideration of the microscopic structures of the two solvents in the close vicinity of the different ions. Spatial correlations can be analyzed by computing the corresponding solute-solvent, site-site pair correlation functions, namely,

$$g_{ion\,\alpha}(r) = \frac{1}{4\pi r^2 \rho_{\alpha}} \sum_i \left\langle \delta\left(\left|\mathbf{r}_i^{\alpha} - \mathbf{r}^{ion}\right| - r\right)\right\rangle, \tag{8}$$

where ρ_{α} is the density of the species α and $\langle\cdots\rangle$ denotes an equilibrium ensemble average. In the present context, it is also instructive to compute cumulative integrals of the type

$$n_{\alpha}(r) = \rho_{\alpha} \int_0^r g_{ion\,\alpha}(r')\, \mathrm{d}\mathbf{r}', \tag{9}$$

which provide estimates for the number of solvent sites which lie within a distance r from the solute.

Results for $g_{\mathrm{Li}^+\alpha}(r)$ and $n_{\alpha}(r)$ for some relevant solvent sites in different mixtures are presented in Fig. 1, while the corresponding functions for K^+ are depicted in Fig. 2. All Li^+–O profiles exhibit prominent main peaks located at $r \sim 1.9$ Å revealing strong local density fluctuations and a clear preferential solvation of the cation by DMSO. As such,

This article is copyrighted as indicated in the article. Reuse of AIP content is subject to the terms at: http://scitation.aip.org/termsconditions. Downloaded to IP: 157.92.4.6 On: Fri, 05 Dec 2014 14:42:06

TABLE I. Potential parameters for bonded and non-bonded interactions.

DMSO[a]				ACN[b]			
Site	σ (Å)	ϵ (kcal mol^{-1})	$z(e)$	Site	σ (Å)	ϵ (kcal mol^{-1})	$z(e)$
O	3.03	0.120	− 0.556	N	3.25	0.1700	− 0.532
S	3.56	0.350	0.312	C1	3.40	0.0860	0.481
C	3.64	0.078	− 0.148	C2	3.40	0.1094	− 0.479
H	2.39	0.024	0.090	H	2.65	0.0157	0.177
Bond	r_0 (Å)	k_{str} (kcal mol^{-1} Å^{-2})		Bond	r_0 (Å)	k_b (kcal mol^{-1} Å^{-2})	
H–C	1.11	322		N–C1	1.157	600	
C–S	1.80	240		C1–C2	1.458	400	
S–O	1.53	540		C2–H	1.090	340	
Angle	θ_0 (deg)	k_θ (kcal mol^{-1} rad^{-2})		Angle	θ_0 (deg)	k_θ (kcal mol^{-1} rad^{-2})	
H–C–H	108.4	35.5		C2–C1–N	180	80	
H–C–S	111.3	46.1		H–C2–C1	110	35	
C–S–O	106.75	79.0		H–C2–H	109.5	35	
C–S–C	95.0	34.0					
Dihedral	n	k_ϕ (kcal mol^{-1})	δ (deg)				
H–C–S–O	3	0.2	0				
H–C–S–C	3	0.2	0				
Ion	σ (Å)	ϵ (kcal mol^{-1})	$z(e)$				
Li^+	1.39[c]	0.165	1				
K^+	3.33[d]	0.1[d]	1				
Cl^-	4.41[d]	0.1[d]	− 1				

[a]From Ref. 38.
[b]From Ref. 42.
[c]1.506 in the original model, Ref. 44.
[d]From Ref. 46.

we found that it is only as one surpasses, say, $x_{ACN} \sim 0.90$ that the Li^+ first solvation incorporates ACN molecules with meaningful probability. We finally remark that, in the limiting case of pure ACN, the first solvation shell of the cation includes, in average, ∼4.5 molecules. Similar conclusions can be drawn for K^+ solvation, although the magnitude of the ionic-solvent coupling is somewhat milder. Compared to the Li^+ case, the spatial correlations depicted in Fig. 2 show that the first solvation shell moves ∼1 Å away from the cation and is composed exclusively of ∼6–7 DMSO molecules, for concentrations $x_{ACN} \lesssim 0.75$. Contrasting, spatial correlations involving chloride solutions (not shown), reveal that, as expected from simple electrostatic considerations, the solvent sites lying at the close vicinity of anions are the methyl groups of both solvents. Moreover, shell populations vary linearly with global concentrations along the whole composition range, with limiting values $n_{CH_3^{ACN}} = 10$ and $n_{CH_3^{DMSO}} = 12$ for the corresponding pure solvents.

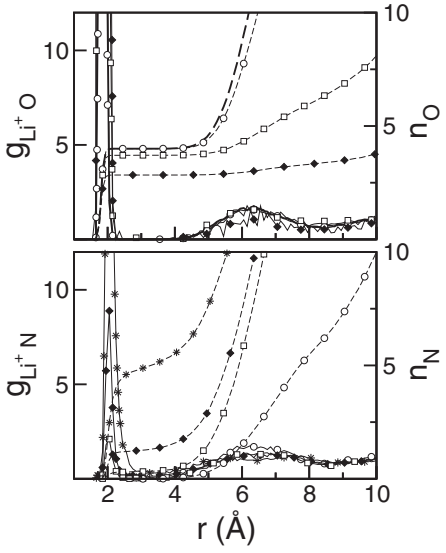

FIG. 1. Solute-solvent, site-site pair correlation functions, and cumulative integrals for Li^+ in different DMSO-ACN mixtures. $x_{ACN} = 0$ (solid line), $x_{ACN} = 0.25$ (open circles), $x_{ACN} = 0.9$ (open squares), $x_{ACN} = 0.97$ (black diamonds), $x_{ACN} = 1$ (stars).

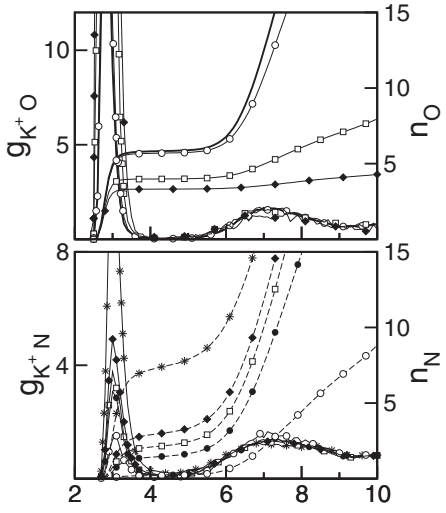

FIG. 2. Same as Fig. 1 for K^+.

This article is copyrighted as indicated in the article. Reuse of AIP content is subject to the terms at: http://scitation.aip.org/termsconditions. Downloaded to IP: 157.92.4.6 On: Fri, 05 Dec 2014 14:42:06

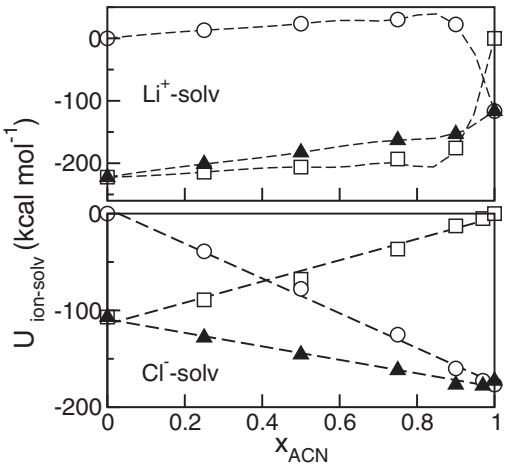

FIG. 3. Ion-solvent interaction energy as a function of composition (black triangles). Also shown are the individual solvent contributions: DMSO (open squares) and ACN (open circles). Dashed lines were added as a guide to the eye.

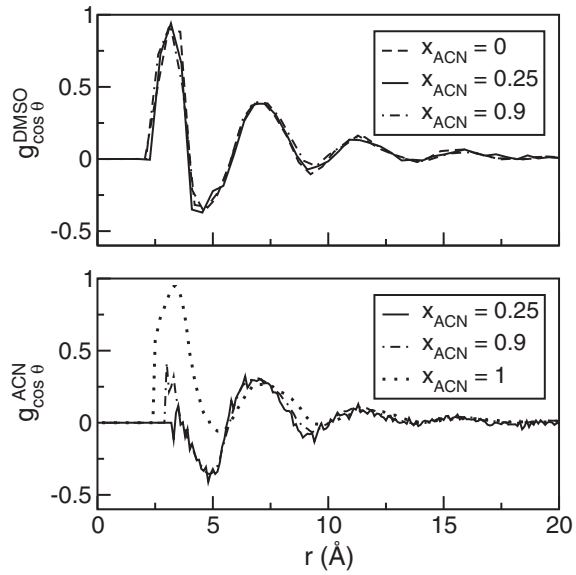

FIG. 4. Orientational correlations for the individual solvents $g^{\gamma}_{\cos\theta}$ in the different solvation shells of Li^+(see text). Upper panel: DMSO; lower panel: ACN. Dashed lines were added as a guide to the eye.

In the present context, it will be instructive to analyze the different scenarios from a complementary, energetic perspective. To that end, we computed the total solute-solvent average potential energy $U_{ion-solv}$, namely,

$$U_{ion-solv} = \sum_{\alpha} \rho_{\alpha} \int_0^{\infty} g_{ion\,\alpha}(r)\, u_{ion\,\alpha}(r)\, \mathrm{d}\mathbf{r}. \qquad (10)$$

Results for $U_{ion-solv}$ as a function of the solvent composition are depicted in Fig. 3. In the upper panel, one observes that, starting from the pure DMSO result, $U_{\mathrm{Li^+DMSO}} \sim -220$ kcal mol^{-1}, the solute-solvent energy looks fairly linear except across a narrow concentration interval, $0.95 \lesssim x_{\mathrm{ACN}} \lesssim 1$, where the plot presents a sharp increment, before attaining $U_{\mathrm{Li^+ACN}} \sim -150$ kcal mol^{-1} for the pure ACN limit.

The decomposition of the previous energetic results into contributions from the individual solvents (also shown in Fig. 3) is also interesting. Note that the DMSO contribution is the dominant one and is strongly negative, whereas the ACN one is approximately four times smaller and positive, except for the pure ACN case. The fact that the DMSO contribution prevails over the ACN one, even in solutions where $x_{\mathrm{ACN}} \sim 20 \times x_{\mathrm{DMSO}}$, is striking, and would corroborate that the dominant fraction of solute-solvent coupling is provided by the closest solvation shell. A similar energetic analysis performed in K^+ solutions (not shown) leads to similar conclusions. A sharp contrast is found in the analysis of the composition dependence of the different contributions to the Cl^--solvent coupling shown in the bottom panel of Fig. 3. Not only do the three plots exhibit fairly linear concentration dependences, but also the two individual contributions to the solute-solvent coupling are negative.

The presence of a positive ACN contribution in the Li^+-solvent coupling is somewhat puzzling. This would suggest that the resulting structures of the closest shells are not just the ones predicted based on the characteristics of the ionic Coulomb field, but it is in fact the result of a complex interplay in which solvent-solvent interactions also play a key role. In order to shed light on the reasons of the resulting spatial arrangements, we analyzed local solvent orientational correlations in the close vicinity of the solute via the following conditional probability distribution function:

$$g^{\gamma}_{\cos\theta}(r) = \frac{\left\langle \sum_i \delta(r - r_i) \cos\theta_i^{\gamma} \right\rangle}{\left\langle \sum_i \delta(r - r_i) \right\rangle}. \qquad (11)$$

In the previous equation, the angle θ_i^{γ} is given by

$$\cos\theta_i^{\gamma} = \frac{\left(\mathbf{R}_i^{\gamma} - \mathbf{r}^{\mathrm{Li^+}}\right) \cdot \boldsymbol{\mu}_i^{\gamma}}{\left|\mathbf{R}_i^{\gamma} - \mathbf{r}^{\mathrm{Li^+}}\right| \left|\boldsymbol{\mu}_i^{\gamma}\right|}, \qquad (12)$$

where $\boldsymbol{\mu}_i^{\gamma}$ and $\mathbf{R}_i^{\gamma}$ represent the dipole moment and the coordinate of the center of mass of the ith molecule of species γ = ACN, DMSO.

Results of $g^{\gamma}_{\cos\theta}(r)$ appear in Fig. 4. The plot for DMSO shows that the closest shell responds to the ionic Coulomb coupling by orienting their dipoles parallel to the solute electric field, i.e., $\cos\theta_{\mathrm{DMSO}}(r = 3\,\text{Å}) \sim 0.7$–$0.95$. Contrasting, the dipole alignment of the closest ACN molecules lying at $r \sim 5$ Å turns out to be slightly anti-parallel, i.e., $\cos\theta_{\mathrm{ACN}}$ $(r = 5\,\text{Å}) \sim -0.4$. In both cases, local orientations beyond the first solvation shells present alternance of parallel and antiparallel alignments.

One can rationalize this structure by analyzing charge distributions in the molecules of the two solvents: the entries in Table I show that, in DMSO, charge separation prevails mostly along the distal O–S bond regions since the excess local charge density at each of the "hydrophobic," methyl groups barely exceeds $\sim 0.05e$. As such, at distances of the order of $r \gtrsim \sigma_{\mathrm{Li-O}} + r_0^{\mathrm{O-S}} \sim 4$ Å away from the solute, the local electric field promoted by the excess charge should be significantly shielded by the four, tightly bound, DMSO molecules. Moreover, a close inspection of a large number of solvation structures of ACN in the outer, second solvation shell reveals that the prevailing molecular arrangements are characterized by molecules exposing their "hydrophobic"

This article is copyrighted as indicated in the article. Reuse of AIP content is subject to the terms at: http://scitation.aip.org/termsconditions. Downloaded to IP: 157.92.4.6 On: Fri, 05 Dec 2014 14:42:06

flanks in close contact with the ones of the inner DMSO molecules. Note that this favorable solvent-solvent coupling would lead to negative projections of the ACN dipoles with respect to the ionic electrical field, bringing the ACN contribution to the solute-solvent coupling positive. We remark that the anti-parallel alignment is not restricted to the analysis of binary solutions but has been reported in previous studies dealing with ionic solvation in pure ACN as well.[27,47–49]

The previous energetic analysis can be complemented by examining the relative stabilization of the different ionic solutes with respect to their "uncharged" counterparts. Here, we are referring to free energy differences associated to the following processes in solution:

$$\begin{aligned} \mathrm{M(sol)} &\rightarrow \mathrm{M^{+}(sol)}, \\ \mathrm{X(sol)} &\rightarrow \mathrm{X^{-}(sol)}, \end{aligned} \tag{13}$$

with M = Li, K and X = Cl. In the present case, free energy differences were computed using standard free energy perturbation procedures[50] that involve connecting initial and final states by a series of intermediate states in which solute-solvent Coulomb interactions are controlled by a "coupling parameter" λ, namely,

$$\Delta A = \int_0^1 \mathrm{d}\lambda \sum_\alpha \rho_\alpha \int_0^\infty g_{ion\,\alpha}(r;\lambda)\, u_{ion\,\alpha}(r;\lambda)\, \mathrm{d}\mathbf{r}, \tag{14}$$

where $g_{ion\,\alpha}(r;\lambda)$ represents pair correlation functions evaluated with the solute-solvent Coulomb coupling term in Eq. (7), $u_{ion\,\alpha}(r;\lambda)$ scaled by the parameter λ. For each value of λ, the systems were equilibrated for about 5 ps, and statistics was collected during subsequent 500 ps runs. We implemented the single-topology approach in which the electrostatic interactions were perturbed without modifying the Lennard-Jones terms.[51] To check for appropriate convergence, we run two sets of simulations, starting from λ = 0(1) and by setting Δλ = +(−)0.0625.

Results for Δ*A* as a function of the composition of the aprotic mixture are presented in Fig. 5. One observes much more marked stabilizations of ionic species in DMSO-rich solutions. Moreover, in the two upper panels, the "kinks" and the sharp increments in the slopes, for $x_{\mathrm{ACN}} \sim 0.85$ ($\mathrm{Li^{+}}$) and $x_{\mathrm{ACN}} \sim 0.75$ ($\mathrm{K^{+}}$), contrast markedly with the linear concentration dependence registered for $\Delta A_{\mathrm{Cl^{-}}}$ (bottom panel). Incidentally, we remark that the stabilization of the ionic species observed in DMSO-rich solutions is consistent with the $\Delta E_0 \sim 0.5$ V difference registered between the $\mathrm{Li/Li^{+}}$ oxidation potentials in pure DMSO and in pure ACN.[29] In addition, the analysis of the concentration dependence of the latter oxidation potentials in mixtures shows sharp increments above $x_{\mathrm{ACN}} > 0.8$, suggesting qualitative changes in the overall solvation structures accordant with the ones described here.

The last aspect related to the equilibrium solvation structures that we will analyze deals with the potential of mean force, $W(r)$ for the ionic association of LiCl. $W(r)$ represents the reversible work necessary to bring the cation and the anion from an infinite distance down to a distance *r*. namely,

$$-\beta W(r) \propto \ln\left[\frac{1}{r^2}\langle\delta(r_{\mathrm{X^{-}Li^{+}}} - r)\rangle\right]. \tag{15}$$

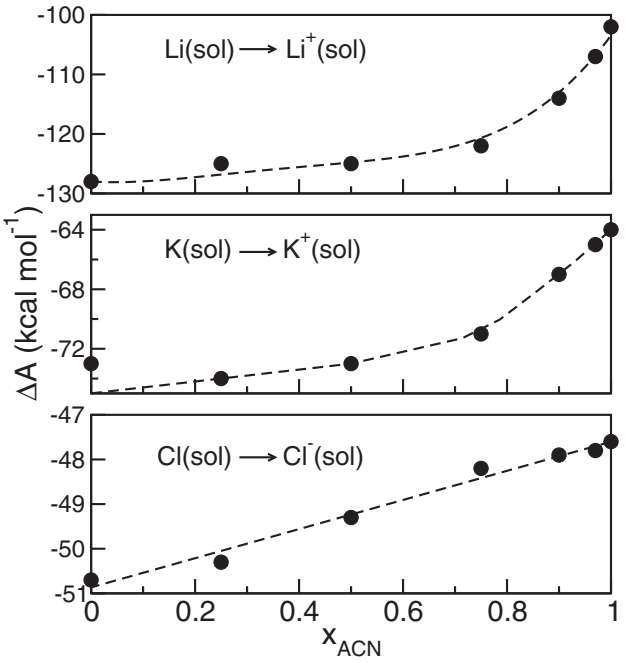

FIG. 5. Free energy associated to the "charging" processes shown in Eq. (13).

In Fig. 6, we show results for the potential of mean force for LiCl in different DMSO-ACN mixtures obtained by implementing an adaptive biasing force scheme.[52] Upon a first inspection, several features are worth commenting: (i) taking as a reference the corresponding dissociated-ion-states, the free energy difference between the corresponding contact-ion-pair (CIP) states in the two solvents is $W_{\mathrm{DMSO}}(r = 2.3\,\text{Å}) - W_{\mathrm{ACN}}(r = 2.3\,\text{Å}) \sim -5$ kcal mole^{-1}. We remark that this trend is consistent with the ∼7 order of magnitude difference reported for the corresponding dissociation constants of the related electrolyte HCl in the two solvents, namely: $[K^d_{\mathrm{HCl}}(\mathrm{DMSO})/K^d_{\mathrm{HCl}}(\mathrm{ACN})]_{\mathrm{exp}} \sim 6.9 \times 10^6$;[53] (ii) second, the ACN profile (black circles) reveals that, in the latter solvent, solvent-separated-ion-pair (SSIP) states are only marginally stable, a fact that has also been registered in a previous simulation study of acid dissociation in ACN;[54] (iii) in a related context, note that the barrier separating SSIP from CIP states – which would be indicative of a tight packing of the DMSO molecules lying in the

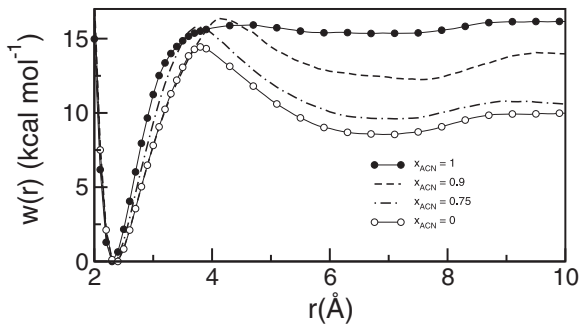

FIG. 6. Potential of mean force for LiCl in different DMSO-ACN mixtures. The curves were shifted to correspond to their first minima.

This article is copyrighted as indicated in the article. Reuse of AIP content is subject to the terms at: http://scitation.aip.org/termsconditions. Downloaded to IP: 157.92.4.6 On: Fri, 05 Dec 2014 14:42:06

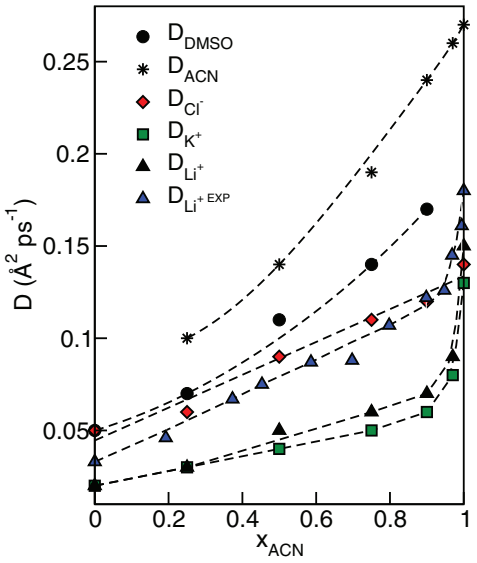

FIG. 7. Diffusion coefficients for different species. DMSO: circles, ACN: stars, Cl^-: red diamonds, K^+: green squares, Li^+: black triangles. Also shown are experimental results for Li^+ (blue triangles) obtained from conductivity measurements.[29]

interionic region – remains fairly constant along practically the whole composition range, before vanishing in the narrow $x_{ACN} \gtrsim 0.9$ concentration interval.

To conclude our analysis, we will briefly comment on dynamical aspects related to the ionic transport in the binary mixtures. In Fig. 7, we present results for diffusion coefficients for the solvents and the different solutes. The data were obtained from the corresponding mean square displacements, namely,

$$D_\alpha = \frac{1}{6} \lim_{t\to\infty} \frac{\mathrm{d}\langle|\mathbf{r}^\alpha(t) - \mathbf{r}^\alpha(0)|^2\rangle}{\mathrm{d}t}. \tag{16}$$

The solvent diffusion constants are in good agreement with the values reported by Bernardi and Stassen[43] and reveal that the overall translational dynamics of the two components become faster in ACN-rich solutions. Concerning the cations, the corresponding diffusion constants are practically one order of magnitude smaller than those observed for the solvents, a fact that could be ascribed to concerted translations of much more massive moieties involving the tagged solutes plus their first coordination shells. Contrasting, the values of D_{Cl^-} compare much more favorably with the ones computed for the individual solvent species, whereas the corresponding concentration dependence looks fairly linear. The latter features, in turn, would be consistent with smaller solute-solvent effective couplings and the absence of preferential solvation by either solvent.

In Fig. 7, we have also included results from conductivity measurements recently reported by Mozhzhukhina *et al.* (blue triangles).[29] The Li^+ diffusion coefficient was estimated from the corresponding conductivity, $\lambda^\circ_{Li^+}$,

$$\lambda^\circ_{Li^+} = \Gamma^\circ(LiPF_6) - (1 - t_+)\Gamma^\circ(TBAPF_6). \tag{17}$$

In the previous equation, $\Gamma^\circ(MX)$ represents the limiting conductivity of the MX electrolyte ($M^+ = Li^+$, tetrabutylammonium) and ($X^- = PF_6^-$) whereas $t_+ = 0.36$ represents the average transport number of TBA^+ in $TBAPF_6$ solutions.[55] The Einstein relationship establishes the correspondence between conductivities and the diffusion coefficients, namely,

$$D_i = \frac{\lambda_i^\circ}{\beta N_A e^2}, \tag{18}$$

where N_A and e represent the Avogadro number and the charge of the electron.

Compared to the experimental results, our simulation predictions exhibit a consistent underestimation along the whole concentration interval, which can be attributed to inherent deficiencies in the parametrization of the adopted Hamiltonian. Nonetheless, we would like to remark the similarities in the concentration trends of both sets of data, i.e., a linear behavior at low ACN contents followed by sharper increments in a narrow concentration regime beyond, say, $x_{ACN} = 0.90$.

IV. CONCLUDING REMARKS

The results presented in this paper shed light on microscopic characteristics of the solvation of simple ionic species in aprotic mixtures combining DMSO and ACN. Special emphasis has been put in describing the solvation of Li^+, due to its potential relevance in the development of advanced Li-air batteries. In this context, the present results provide additional insights for the correct interpretation of a series of recent experimental measurements.[18,29] One important conclusion that can be drawn from our simulations is related to the marked asymmetry between the prevailing solvation structures of anions and cations. The preferential solvation of cations by DMSO is clearly demonstrated by the constancy in the compositions of the first solvation shells of Li^+ and K^+, which include exclusively DMSO molecules, down to concentrations close to $x_{DMSO} \sim 0.1$. This feature is also manifested in the bimodal concentration dependences of two relevant thermodynamic quantities pertaining to the solvation processes: (i) the solvent-solute energy coupling and (ii) the relative stabilization of ionic species, compared to their electrically neutral counterparts. Starting from the pure DMSO case, concentration trends for the energetics exhibit nearly linear behaviors, down to mixtures with concentrations comparable to the above mentioned value, i.e., $x_{DMSO} \sim 0.1$. Below the latter DMSO concentration range, the curves present sharp modifications before reaching the limiting, pure-ACN limit. Contrasting, the scenarios for the anion-solvation differ at a qualitative level and can be cast in terms of more uniform, simpler linear models. Moreover, the relative stabilization of ionic species compared to their electrically neutral counterparts presents a steady increment with the relative content of DMSO that also explains the differences registered in the association processes of LiCl in these solutions in a natural fashion.

The previous description clearly underlines the complexity of the interplay that exists between the roles played by ion-solvent and solvent-solvent interactions, as controlling agents of the resulting solvation structures. Note that, in principle, at the crudest level of description, the two solvents could be categorized as exhibiting "similar" physico-chemical properties,

This article is copyrighted as indicated in the article. Reuse of AIP content is subject to the terms at: http://scitation.aip.org/termsconditions. Downloaded to IP: 157.92.4.6 On: Fri, 05 Dec 2014 14:42:06

such as their common aprotic character and comparable dipolar moments, to cite two relevant examples within the present context. Yet, differences in the overall molecular geometries and charge distributions are sufficient to promote important unbalances in the magnitudes of their individual responses stabilizing ionic species in these polar mixtures. More importantly, our simulations also reveal that the consideration of these competitive effects is essential to achieve correct physical interpretations not only of equilibrium aspects of the solvation but of the ionic transport as well.

We are confident that the previous conclusions will deepen the understanding of ionic processes involved in the operation of Li-air batteries that might incorporate aprotic mixtures as solvent media. A molecular level analysis of Li^+ solvation in mixtures which are amenable to a direct simulation approach is relevant for the rational design of electrolytes in lithium-oxygen battery cathodes. More specifically, the structural characteristics of the Li^+ solvation play a key role in the stabilization of intermediates of Oxygen reduction reactions, such as lithium superoxide or peroxide. As such, the present analysis brings about the possibility to look at these solvation effects with solvents which combine different abilities to coordinate lithium ions and to dissolve oxygen. Still, we foresee the necessity of additional research before an optimal choice can be identified.

ACKNOWLEDGMENTS

D.L. and E.J.C. are permanent research staff of CONICET-Argentina. NAMD was developed by the Theoretical and Computational Biophysics Group in the Beckman Institute for Advanced Science and Technology at the University of Illinois at Urbana-Champaign. Financial support from CONICET, the University of Buenos Aires, and ANCyPT is greatly acknowledged.

[1]B. Scrosati and J. Garche, J. Power Sources **195**, 2419 (2010).
[2]A. Kraytsberg and Y. Ein-Eli, J. Power Sources **196**, 886 (2011).
[3]G. Girishkumar, B. McCloskey, A. C. Luntz, S. Swanson, and W. Wilcke, J. Phys. Chem. Lett. **1**, 2193 (2010).
[4]K. M. Abraham and Z. A. Jiang, J. Electrochem. Soc. **143**, 1 (1996).
[5]K. Xu, Chem. Rev. **104**, 4303 (2004).
[6]D. G. Kwabi, N. Ortiz-Vitoriano, S. A. Freunberger, Y. Chen, N. Imanishi, P. G. Bruce, and Y. Shao-Horn, MRS Bull. **39**, 443 (2014).
[7]N. Garcia-Araez and P. Novák, J. Solid State Electrochem. **17**, 1793 (2013).
[8]M. D. Bhatt, H. Geaney, M. Nolan, and C. O'Dwyer, Phys. Chem. Chem. Phys. **16**, 12093 (2014).
[9]A. Khetan, H. Pitsch, and V. Viswanathan, J. Phys. Chem. Lett. **5**, 1318 (2014); **5**, 2419 (2014).
[10]V. S. Bryantsev, J. Uddin, V. Giordani, W. Walker, D. Addison, and G. V. Chase, J. Electrochem. Soc. **160**, A160 (2013).
[11]V. S. Bryantsev, V. Giordani, W. Walker, M. Blanco, S. Zecevic, K. Sasaki, J. Uddin, D. Addison, and G. V. Chase, J. Phys. Chem. A **115**, 12399 (2011).
[12]J. Lu, L. Li, J.-B. Park, Y.-K. Sun, F. Wu, and K. Amine, Chem. Rev. **114**, 5611 (2014).
[13]N. Imanishi and O. Yamamoto, Mater. Today **17**, 24 (2014).
[14]D. Xu, Z. Wang, J. Xu, L. Zhang, and X. Zhang, Chem. Commun. **48**, 6948 (2012).
[15]Z. Peng, S. A. Freunberger, Y. Chen, and P. G. Bruce, Science **337**, 563 (2012).
[16]D. Sharon, M. Afri, M. Noked, A. Garsuch, A. A. Frimer, and D. Aurbach, J. Phys. Chem. Lett. **4**, 3115 (2013).
[17]B. D. McCloskey, A. Valery, A. C. Luntz, S. R. Gowda, G. M. Wallraff, J. M. Garcia, T. Mori, and L. E. Krupp, J. Phys. Chem. Lett. **2**, 1161 (2011).
[18]E. J. Calvo and N. Mozhzhukhina, Electrochem. Commun. **31**, 56 (2013).
[19]E. Pasgreta, R. Puchta, M. Galle, N. van Eikema Hommes, A. Zahl, and R. van Eldik, ChemPhysChem. **8**, 1315 (2007).
[20]E. Pasgreta, R. Puchta, A. Zahl, and R. van Eldik, Eur. J. Inorg. Chem. **2007**, 1815 (2007).
[21]T. Megyes, I. Bakó, T. Radnai, T. Gróz, T. Kosztolányi, B. Mroz, and M. Probst, Chem. Phys. **321**, 100 (2006).
[22]D. M. Seo, P. D. Boyle, O. Borodin, and W. A. Henderson, RSC Adv. **2**, 8014 (2012).
[23]J. Barthel and R. Deser, J. Sol. Chem. **23**, 1133 (1994).
[24]O. N. Kalugin, A. K. Adya, M. N. Volobuev, and Y. V. Kolesnik, Phys. Chem. Chem. Phys. **5**, 1536 (2003).
[25]U. Onthong, T. Megyes, I. Bakó, T. Radnai, K. Hermansson, and M. Probst, Chem. Phys. Lett. **401**, 217 (2005).
[26]W. Kunz, J. Barthel, L. Klein, T. Cartailler, P. Turq, and B. Reindl, J. Sol. Chem. **20**, 875 (1991).
[27]D. Spångbeg and K. Hermansson, Chem. Phys. **300**, 165 (2004).
[28]D. M. Seo, O. Borodin, S.-D. Han, P. D. Boyle, and W. A. Henderson, J. Electrochem. Soc. **159**, A1489 (2012).
[29]N. Mozhzhukhina, M. P. Longinotti, H. R. Corti, and E. J. Calvo, "A conductivity study of preferential solvation of lithium ion in acetonitrile-dimethyl sulfoxide mixtures," Electrochim. Acta (in press).
[30]R. J. Fort and W. R. Moore, Trans. Faraday Soc. **61**, 2102 (1965).
[31]L. Martínez, R. Andrade, E. G. Birgin, and J. M. Martínez, J. Comput. Chem. **30**, 2157 (2009).
[32]T. A. Darden, D. M. York, and L. G. Pedersen, J. Chem. Phys. **98**, 10089 (1993); U. Essmann, L. Perera, M. L. Berkowitz, T. A. Darden, H. Lee, and L. G. Pedersen, *ibid.* **103**, 8577 (1995).
[33]J. C. Phillips, R. Braun, W. Wang, J. Gumbart, E. Tajkhorshid, E. Villa, C. Chipot, R. D. Skeel, L. Kale, and K. Schulten, J. Comput. Chem. **26**, 1781 (2005).
[34]A. Luzar and D. Chandler, J. Chem. Phys. **98**, 8160 (1993).
[35]H. Liu, F. Müller-Plathe, and W. F. van Gunsteren, J. Am. Chem. Soc. **117**, 4363 (1995).
[36]M. Skaf, J. Chem. Phys. **107**, 7996 (1997).
[37]I. Benjamin, J. Chem. Phys. **110**, 8070 (1999).
[38]M. Strader and S. E. Feller, J. Phys. Chem. A **106**, 1074 (2002).
[39]P. Bordat, J. Sacristan, D. Reith, S. Girard, A. Glättli, and F. Müller-Plathe, Chem. Phys. Lett. **374**, 201 (2003).
[40]X. Grabuleda, C. Jaime, and P. A. Kollman, J. Comput. Chem. **21**, 901 (2000).
[41]E. Guàrdia, R. Pinzón, J. Casulleras, M. Orozco, and F. J. Luque, Mol. Simul. **26**, 287 (2001).
[42]A. M. Nikitin and A. P. Lyubartsev, J. Comput. Chem. **28**, 2020 (2007).
[43]E. Bernardi and H. Stassen, J. Chem. Phys. **120**, 4860 (2004).
[44]L. X. Dang, J. Chem. Phys. **96**, 6970 (1992).
[45]M. P. Allen and D. J. Tildesley, *Computer Simulation of Liquids* (Clarendon, Oxford, 1987).
[46]E. Guàrdia, D. Laria, and J. Martí, J. Phys. Chem. B **110**, 6332 (2006).
[47]J. Richardi, P. H. Fries, and H. Krienke, J. Chem. Phys. **108**, 4079 (1998).
[48]E. Guàrdia and R. Pinzón, J. Mol. Liq. **85**, 33 (2000).
[49]R. Fischer, J. Richardi, P. H. Fries, and H. Krienke, J. Chem. Phys. **117**, 8467 (2002).
[50]D. Chandler, *Introduction to Modern Statistical Mechanics* (Oxford University Press, Oxford, 1987), Chap. 7.
[51]S. B. Dixit and C. Chipot, J. Phys. Chem. A **105**, 9795 (2001); C. Chipot and D. A. Pearlman, Mol. Simul. **28**, 1 (2002); C. Chipot and A. Pohorille, *Free Energy Calculations: Theory and Applications in Chemistry and Biology* (Springer Verlag, Berlin, 2007).
[52]E. Darve and A. Pohorille, J. Chem. Phys. **115**, 9169 (2001); D. Rodriguez-Gomez, E. Darve, and A. Pohorille, *ibid.* **120**, 3563 (2004); J. Hénin and C. Chipot, *ibid.* **121**, 2904 (2004).
[53]I. M. Kolthodd, S. Bruchenstein, and M. K. Chantooni, Jr., J. Am. Chem. Soc. **83**, 3927 (1961); C. Cooke, C. McCallum, A. D. Pethybridge, and J. E. Prue, Electrochim. Acta **20**, 591 (1975).
[54]D. Laria, R. Kapral, D. Estrin, and G. Ciccotti, J. Chem. Phys. **104**, 6560 (1996).
[55]D. L. Goldfarb, M. P. Longinotti, and H. R. Corti, J. Sol. Chem. **30**, 307 (2001); N. G. Tsierkezos and A. I. Philippopoulos, Fluid Phase Equilib. **277**, 20 (2009).

This article is copyrighted as indicated in the article. Reuse of AIP content is subject to the terms at: http://scitation.aip.org/termsconditions. Downloaded to IP: 157.92.4.6 On: Fri, 05 Dec 2014 14:42:06